International Journal of Heat and Technology
Vol. 44, No. 2, April, 2026, pp. 537-550
Journal homepage: http://iieta.org/journals/ijht

Optimization of Combined Cooling, Heating, and Power Systems with Integrated Solar Collectors for Enhanced Thermal and Energy Performance

Mohammed Salam Abdulghafoor, Mohammed K. Al-Saadi, Ameer Abed Jaddoa*

Electromechanical Engineering Department, University of Technology, Baghdad 00964, Iraq

Corresponding Author Email: Ameer.A.Jaddoa@uotechnology.edu.iq

https://doi.org/10.18280/ijht.440209

Received: 5 August 2025
Revised: 20 January 2026
Accepted: 2 February 2026
Available online: 30 April 2026

Keywords:
combined heat, power and cool, unit commitment, micro grids, mixed integer non-liner programming, solar air heater

ABSTRACT

The increasing demand for low carbon, efficient energy systems in integrated energy applications is addressed in this paper. The potential of combined cooling, heating, and power (CCHP) systems to lower emissions and increase overall energy efficiency has drawn more attention. The optimal operation of the CCHP smart system is developed and proposed in this paper, where the optimization approach is formulated as multi objective mixed integer nonlinear program (MOMINLP). A solar air heater (SAH) is designed and implemented, and then it is experimentally tested. Different designs of the SAH are considered and integrated with the proposed CCHP system to investigate its effect on the optimal operation of the CCHP system. GAMS software is used to create the model, which is then solved to reduce overall operating costs while taking environmental and technological limitations into account. The unit commitment (UC) strategy is developed to react to both the electric and heat systems. Besides, practical limitations are included to bring the problem closer to the actual situation. Many current projects do not fully utilize the combination of solar heating and the best operating techniques to reduce expenses and emissions at the same time. In addition, renewable energy (RE) sources in both electric and heat grids are utilized as well. The results demonstrate that the proposed system significantly reduces carbon emissions and operational expenses in comparison to traditional arrangements under various operating conditions, where using SAH in this way resulted in a 27.8% reduction in the overall cost. These findings highlight the effectiveness of the proposed CCHP configuration in enhancing energy efficiency and sustainability. The novelty of this work lies in demonstrating that optimized CCHP design may drastically lower carbon emissions and operational costs when compared to traditional CCHP systems.

1. INTRODUCTION

Various environmental and ecological problems have arisen as a result of the growing use of energy worldwide, and this is why there is a bad effect on the environment, causing global warming [1]. Conventional combined cooling, heating, and power (CCHP) systems rely on natural gas as their main energy source, making it difficult to optimize the benefits of energy conservation and pollution reduction [2, 3]. The CCHP system integrates several energy supply sources and permits the progressive use of energy [4]. There is an urgent need to optimize the energy system and create a more ecological and ecologically friendly energy system, given the effects of energy consumption and greenhouse gas emissions on human society [5].

The CCHP system of linked solar, biomass, wind, geothermal, and other renewable energy (RE) sources has been the subject of extensive research in recent years [6]. This requires a control technology to distribute capacities and loads between these systems. Building a microgrid within the main network that places energy sources near the end user to meet their demands is one of the creative solutions to this challenge [7-12]. Micro grid MG is a low-voltage distribution network with autonomous control that may be used in both linked to the grid and isolated (island) modes. Distributed generation (DG), micro turbines (MT), and RE are just a few of MG's numerous power sources. Energy storage technologies are also in place to maximize resource utilization and guarantee that the real need for response is met [13]. The integration of RE sources with the grid is problematic because of their stochastic nature and the unpredictability of demand. In addition, the peak periods for the generation of energy from renewable sources occur during periods of low loads, which compromises the grid's stability [14]. In addition to the electrical system, MG may contain a heat system known Combined heat and Power micro grid CHP-MG to response to the demand for heat by heat sources, and utilizing of solar energy for heating applications away from electricity generation by using solar air heaters (SAHs) or solar collector, many optimization techniques, including unit commitment (UC), heuristic algorithms, genetic algorithms (GA), particle swarm optimization (PSO), and others, were employed to lower costs and emissions while enhancing the dependability and stability of electricity networks [15], as well as recycling the waste heat that is emitted during the energy generation process for use in heating systems and other uses [16-22].

For example, Ma et al. [23] suggested an interval scheduling technique for CCHP systems with connected solar energy in order to maximize system performance in their study of these systems. In order to compare the CCHP system and the annual total cost-saving rate (ATCSR) under an electrical tracking approach, Jia et al. [24] created a unique CCHP system that combines an organic Rankine cycle with a solar thermal (ST). In addition to the application of CCHP, Soheyli et al. [25] suggested a CCHP system using solid oxide fuel cells (FCs), wind turbines, and photovoltaic (PV) cells as prime movers. They used a multi-objective PSO technique to find the ideal quantity of each system component. In the same construction system in previous literature [26], a hybrid CCHP system for three buildings under various operation methods was optimized and compared. In system B, a photovoltaic thermal solar collector (PVT) transforms solar energy into thermal and electrical energy, while in system A, ST and PV turn solar energy into heat and electricity, respectively. Ge et al. [27] developed three scenarios with various designs and examined their optimal configurations for a solar-assisted natural gas-distributed energy system with energy storage. The findings indicate that the ATCs of the solar-powered DES (scenario 2) and the solar-assisted natural gas DES with energy storage (scenario 3) are reduced by 2.90% and 7.48%, respectively, as compared to the traditional DES (scenario 1).

However, Stanek et al. [28] suggested a CCHP system with a solar power plant and a methane combustion engine. In order to reduce the operating costs of an energy system that consists of CCHP, PV, and storage systems to create a more sustainable energy conversion system, Ruan et al. [29] introduced a unique operational strategy optimization model based on deep reinforcement learning. The TD3 method's performance is on par with the theoretical benchmark, with an average inaccuracy of about 5%.

Song et al. [30] combined geothermal and solar energy, two forms of RE, with the power system to make it possible to generate power using RE. According to the findings, the linked power station's thermal efficiency is 11.21% higher than that of the solo air-cooled geothermal ORC power station.

Our work, a microgrid's energy management approach, was suggested, primarily integrating CCHP-MG with renewable sources in order to satisfy electrical, thermal, and cooling demands. A power MG, micro-Electric system, micro-heat system, and micro-cool system make up the CCHP. MT, FC, gas boiler (GB), electric heater (EH), electric chiller (EC), absorption chiller (AC), and P2G technology are the means by which these systems connect with one another, in addition to renewable sources such as wind turbine (WT), solar air heater (SAH), and Photovoltaic (PV). This was put into practice to ascertain which design offers the system's lowest operating costs. The system was also linked to the utility grid, allowing for constant interchange. GAMS software was used to integrate the exchange power in MG with a methodology of Mixed-Integer Non-Linear Programming MINLP during 24 hours. The novelty of this work lies in the development of an optimization that reduces operational expenses and carbon emissions while taking into account specific technological and environmental restrictions, which makes this study distinctive. may greatly increase energy efficiency and accomplish considerable cost and emission savings.

Therefore, this study builds an optimization-based CCHP model integrated with solar heating to effectively address the economic and environmental limitations of traditional CCHP systems.

2. MODELING OF SYSTEM'S COMPONENTS

Figure 1 depicts the CCHP's suggested structure. A power MG, micro-gas system, micro-heat system, and micro-cool system make up the CCHP. The CCHP uses MT, FC, GB, EH, EC, AC, and P2G technology to facilitate communication between these systems. Natural gas powers the CHP-based MT, which concurrently produces power and heat. The FC converts the natural gas to power, the GB turns it into heat, and the EH uses the energy to produce heat. Additionally, AC turns heat into cool, whereas EC turns electricity into cooling the P2G system. The MG provides the power after CO_2 is extracted from CHP and combined with H2 to create synthetic natural gas (SNG). By lowering CO_2 emissions into the atmosphere, this procedure lessens environmental harm [1, 31-33].

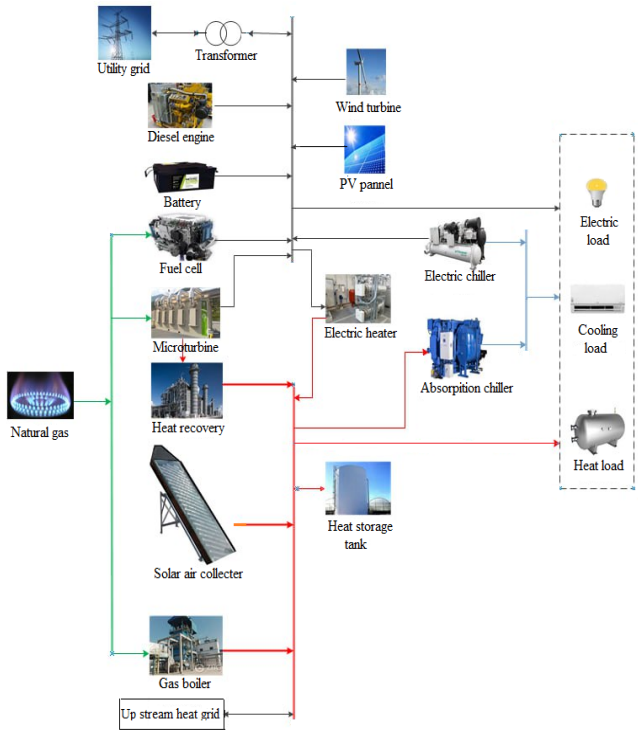

Figure 1. Schematic diagram of combined cooling, heating, and power (CCHP) microgrid

2.1 Heat recovery model

Heat recovery (HR), also known as CHP, is utilized in this study to recover lost heat when electrical power is produced from a microturbine. HR or microturbine heat: H_{MT}^{t} in KW may be written as follows:

$$H_{MT}^{t} = \frac{P_{MT}^{t}\,(1-\eta_{MT}-\eta_{l})\eta_{HR}}{\eta_{MT}} \tag{1}$$

where, η_l is the heat loss factor, η_{HR} is the efficiency of HR.

2.2 Diesel generator model

Diesel generator (DG) is an internal combustion diesel fuel generator used in this study to generate power during peak hours. The fuel consumption may be represented by the following linear equation: P_{DG}^{t} is the output electrical power

from FC at each time in (KWh), η_{DG} is the efficiency of DG, and C_{DG} is the cost of fuel consumption by using DG in $ [34].

$$C_{DG}{}^{t} = a\,P_{DG}^{t\,2} + b\,P_{DG}^{t} + c \tag{2}$$

The cost coefficient of DG is represented by a, b, and c in $(\frac{\$}{KW^2h})$, $(\frac{\$}{KWh})$, $(\frac{\$}{h})$ correspondingly. One may calculate the start-up cost SUC_{DG} and shut-down cost SDC_{DG} in $ by:

$$SUC_{DG}{}^{t} = Sc_{DG}(U_{DG}^{t} - U_{DG}^{t} * U_{DG}^{t-1}) \tag{3}$$

$$SDU_{DG}^{t} = Sd_{DG}(U_{DG}^{t-1} - U_{DG}^{t} * U_{DG}^{t-1}) \tag{4}$$

The battery's limitation capacity can be stated as follows:

$$P_{DG}^{min}\ U_{DG}^{t} \le P_{b.ch}^{t} \le P_{DG}^{max}\ U_{DG}^{t} \tag{5}$$

where, P_{DG}^{min},P_{DG}^{max} and the U_{DG} on/off state of DG are the lowest and greatest power that DG may produce in KW. and Ramp up limit UR_{DG} and ramp down limit DR_{DG} in KW should be the ramp rate limitation for FC at each time interval.

$$P_{DG}^{t} - P_{DG}^{t-1} \le UR_{DG} \tag{6}$$

$$P_{DG}^{t-1} - P_{DG}^{t} \le DR_{DG} \tag{7}$$

Based on the maintenance cost rate coefficient $K_{om.DG}$ in $(\frac{\$}{KWh})$, the maintenance cost of DG $C_{om.FC}$.

$$C_{om.DG}^{t} = P_{DG}^{t} *\ K_{om.DG} \tag{8}$$

2.3 Microturbines model

The users receive heat and power from the MT-based CCHP unit. The micro-turbine is used as a CHP device. It is powered by natural gas, where using the nanoparticles with fuel lowers greenhouse gas emissions. The following formula is used to determine the gas usage. can be represented by the linear formula [36]:

$$C_{MT}^{t} = \frac{P_{MT}^{t}}{LCV * \eta_{MT}} * \beta_g \tag{9}$$

where, LCV was the low heating value of natural gas $(\frac{KWh}{m^3})$, βg is the price of natural gas $(\frac{\$}{m^3})$, P_{MT}^{t} is the output electrical power from MT at each time in KWh, and C_{MT} is the cost of fuel consumption by the utilized microturbine in $.

It is possible to tune, the start-up cost SUC_{MT} and shut-down cost SDC_{MT} in ($) by:

$$SUC_{MT}{}^{t} = Sc_{MT}(U_{MT}^{t} - U_{MT}^{t} * U_{MT}^{t-1}) \tag{10}$$

$$SDC_{MT}{}^{t} = Sd_{MT}(U_{MT}^{t-1} - U_{MT}^{t} * U_{MT}^{t-1}) \tag{11}$$

The maintenance cost of MT $C_{om.MT}$ base on maintenance cost rate coefficient $K_{om.MT}$ in $(\frac{\$}{KWh})$.

$$C_{om.MT}^{t} = P_{MT}^{t} *\ K_{om.MT} \tag{12}$$

The microturbine's constraint capacity can be stated as follows:

$$P_{MT}^{min}\ U_{MT}^{t} \le P_{MT}^{t} \le P_{MT}^{max}\ U_{MT}^{t} \tag{13}$$

where, P_{MT}^{min}, P_{MT}^{max}, and the U_{MT} on/off state of MT represent the lowest and greatest power that MT can produce in KW. Ramp up limit UR_{MT} and Ramp down limit DR_{MT} in KW should be the ramp rate constraints for MT at each time interval.

$$P_{MT}^{t} - P_{MT}^{t-1} \le UR_{MT} \tag{14}$$

$$P_{MT}^{t-1} - P_{MT}^{t} \le DR_{MT} \tag{15}$$

2.4 Fuel cell model

In this work, chemical energy held in the gas was transformed into electrical energy using a proton membrane FC, which was then employed as a source to generate power. The fuel consumption may be represented using the following linear equation: P_{FC}^{t} is the output electrical power from FC at each time in KWh, η_{FC} is the efficiency of FC, and C_{FC} is the cost of fuel consumption by using FC in $ [35].

$$C_{FC}{}^{t} = \frac{P_{FC}^{t}}{LCV * \eta_{FC}} * \beta_g \tag{16}$$

Both the start-up cost SUC_{FC} and shut-down cost SDC_{FC} in $ can be decided by:

$$SUC_{FC}{}^{t} = Sc_{FC}(U_{FC}^{t} - U_{FC}^{t} * U_{FC}^{t-1}) \tag{17}$$

$$SDC_{FC}{}^{t} = Sd_{FC}(U_{FC}^{t-1} - U_{FC}^{t} * U_{FC}^{t-1}) \tag{18}$$

Based on the maintenance cost rate coefficient $K_{om.FC}$ in $⁄KWh, the maintenance cost of MT $C_{om.FC}$:

$$C_{om.FC}^{t} = P_{FC}^{t} *\ K_{om.FC} \tag{19}$$

The constraint capacity of a microturbine can be expressed by:

$$P_{FC}^{min}\ U_{FC}^{t} \le P_{FC}^{t} \le P_{FC}^{max}\ U_{FC}^{t} \tag{20}$$

where, P_{FC}^{min}, P_{FC}^{max}, and the U_{FC} on/off state of FC represent the lowest and greatest power that FC can produce in KW. and each time interval's ramp rate restriction for FC should be Limits of ramp up UR_{FC} and ramp down DR_{FC} in $.

$$P_{FC}^{t} - P_{FC}^{t-1} \le UR_{FC} \tag{21}$$

$$P_{FC}^{t-1} - P_{FC}^{t} \le DR_{FC} \tag{22}$$

2.5 Electric chiller model

By using cooling electricity, the EC supplies the cooling demand. The following formula represents the EC's output cooling power [31]:

$$Cec(t) = Pec(t)\,.\,COP_{ec} \tag{23}$$

When the electric power provided to EC is represented by $Pec(t)$ and the coefficient of performance is represented by (COP_{ec}).

2.6 Absorber chiller model

By using cooling electricity, the AC supplies the cooling load. The following formula determines the AC's output cooling power:

$$Cac(t) = Hac(t) \,.\, COP_{ac} \tag{24}$$

where, COP_{ac} is the coefficient of performance and $Hac(t)$ is the heat that is given to AC.

2.7 Wind turbine model

Wind turbine power output, expressed P_{WT}^{t} in KW, is correlated with wind speed. In Table 1, the wind power value was taken from the study [35].

2.8 Photo voltage panel model

Utilizing PV panels, PV in this study converts solar radiation into electric power P_{PV}^{t} in KW, which is dependent on solar radiation S in KW/m^2, which was measured in Baghdad in January as shown in Table 1. The P_{PV}^{t} total electrical power product can be written as follows:

$$P_{PV}^{t} = s^{t} * Area\ PV * \eta_{PV} * no.PV \tag{25}$$

2.9 Solar air heater model

A SAH was utilized in this study to transform solar energy into usable thermal energy. Cans of aluminum were set up to examine how they affected performance. The temperature in various sections of the SAH was also measured using a K-type thermocouple, which was connected to an Arduino to provide data to a laptop. As illustrated in Figures 2 and 3. Four research cases and dimensions of AL cans were used that were placed into SAH [36]:

- Case 1: A smooth absorbent plate is used to compare the results.
- Case 2: Longitudinal arrangement of aluminum cans.
- Case 3: Transversely arranged aluminum cans.
- Case 4: A diagonal arrangement of aluminum cans. Case.

The rate of heat transfer for SAH H_{SAH}^{t} in KW can be expressed by [37-39]:

$$H_{SAH}^{t} = m^{\circ} * C_p * (T_o - T_i) \tag{26}$$

whereas, T_o, T_i are the average air outlet and inlet temperatures in C°, C_p is the air specific heat in KJ/Kg*K, and m° is the mass flow rate in the SAH duct in kg/s, the value of H_{SAH}^{t} was measured experimentally for this work in Table 1.

2.10 Electrical heater model

The thermal loads receive heat from the EH, and the output heat H_{EH}^{t} in KW is represented as follows:

$$H_{EH}^{t} = P_{EH}^{t} * \eta_{EH} \tag{27}$$

The constraint capacity of EH can be defined as follows, where η_{EH} is the efficiency of EH and P_{EH}^{t} is the electrical power used to produce heat by EH:

$$H_{EH}^{min}\ U_{EH}^{t} \le H_{EH}^{t} \le H_{EH}^{max}\ U_{EH}^{t} \tag{28}$$

where, U_{EH} is the EH's on/off state and H_{EH}^{min}, H_{EH}^{max} are the lowest and highest power that EH can produce in KW, and EH $C_{om.EK}$ maintenance cost based on the $K_{om.EH}$ maintenance cost rate coefficient in $/KWh.

$$C_{om.EH}^{t} = H_{EH}^{t} *\ K_{om.EH} \tag{29}$$

Table 1. Hourly loads, prices, and renewable generation

Ti (h)	$L_{elctr.}^{t}$ (KWh)	$L_{heat.}^{t}$ (KWh)	$L_{heat.}^{t}$ (KWh)	$\omega_{elect.}^{t}$ $(\frac{\$}{KWh})$	$\omega_{heat.}^{t}$ $(\frac{\$}{KWh})$	P_{WT}^{t} (KW)	S^{t} KW/m^2
t1	192	466.88	87.3	0.01	0.162	55	0
t2	177.6	481.82	61.11	0.018	0.1332	61	0
t3	132	489.29	43.65	0.02	0.1368	65	0
t4	122.4	481.82	26.19	0.018	0.1476	58	0
t5	117.6	489.29	34.92	0.025	0.1008	58	0
t6	110.4	451.94	59.36	0.045	0.054	24	100
t7	162	443.22	78.57	0.1	0.0432	40	210
t8	213.6	428.28	104.8	0.28	0.0972	34	612
t9	258	382.22	96.03	0.45	0.1152	40	665
t10	220.8	343.62	78.57	0.519	0.144	46	788
t11	295.2	336.15	89.57	0.4	0.1116	30	930
t12	368.4	290.09	113.5	0.25	0.09	31	988
t13	442.8	252.74	148.4	0.48	0.054	25	873
t14	421.2	217.88	131	0.3	0.054	25	727
t15	406.8	244.02	109.1	0.25	0.0792	36	630
t16	368.4	282.66	97.77	0.1	0.126	30	325
t17	327.6	367.28	92.56	0.035	0.1476	46	25
t18	339.6	428.28	131	0.045	0.1152	36	0
t19	361.2	520.41	150.2	0.08	0.1008	52	0
t20	420	573.95	157.14	0.12	0.0972	46	0
t21	405.6	559.01	131	0.025	0.1584	52	0
t22	421.2	555.27	104.8	0.015	0.1476	46	0
t23	375.6	539.09	101.3	0.012	0.108	46	0
t24	370.8	520.41	91.7	0.01	0.288	52	0

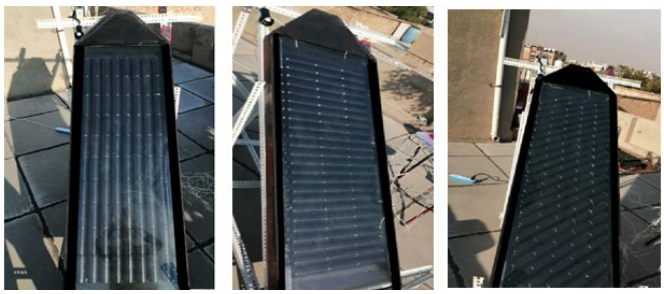

2 3 4

Figure 2. Aluminum cans arranged solar air heaters (SAHs) graph: Case 2 longitudinally; Case 3 transversely; and Case 4 diagonally

Figure 3. Graph of solar air heater (SAH)

2.11 Gas boiler model

Natural gas consumption in the GB produced heat. The cost of natural gas consumption in the GB to produce heat C_{MT} in $ can be stated as follows [40]:

$$C_{GB}{}^{t} = \frac{H_{GB}^{t}}{LCV * \eta_{GB}} * p_g \tag{30}$$

Based on the maintenance cost rate coefficient $K_{om.MT}$ in $/KWh, the maintenance cost of MT $C_{om.MT}$

$$C_{om.GB}^{t} = H_{GB}^{t} * K_{om.GB} \tag{31}$$

The constraint capacity of GB it can be expressed by:

$$H_{GB}^{min} U_{GB}^{t} \le H_{GB}^{t} \le H_{GB}^{max} U_{GB}^{t} \tag{32}$$

where, the U_{GB} on/off state of GB and H_{GB}^{min}, H_{GB}^{max} are the lowest and highest power that FC can produce in KW.

2.12 Energy Storage System model

When energy is plentiful, affordable, or readily available, electrical power is stored for later use using the Energy Storage System (ESS), often known as battery storage. It helps move energy from periods of peak production to periods of high demand for consumption, improving grid stability and dependability. Battery state of charge SOC_b^t in KWh can be written as follows:

$$SOC_b^t = SOC_b^{t-1} - \frac{P_{b.dis}^{t}}{\eta_{b.dis}} + P_{b.ch}^{t}\,\eta_{b.ch} \tag{33}$$

where, η_{ch}, η_{dis} are the charging and discharging battery efficiency and $P_{b.ch}^{t}, P_{b.dis}^{t}$ are the charging and discharging power battery in KWh. The battery's constraint capacity can be stated as follows:

$$P_b^{min} \le P_b^t \le P_b^{max} \tag{34}$$

$$P_{b.ch}^{min} U_{b.ch}^{t} \le P_{b.ch}^{t} \le P_{b.ch}^{max} U_{b.ch}^{t} \tag{35}$$

$$P_{b.dis}^{min} U_{b.ch}^{t} \le P_{b.dis}^{t} \le P_{b.dis}^{max} U_{b.dis}^{t} \tag{36}$$

$$U_{b.dis}^{t} + U_{b.ch}^{t} \le 1 \tag{37}$$

The battery's maximum limit charge and discharge power in KW is denoted by $P_{b.ch}^{min}$, $P_{b.dis}^{min}$, and the minimum limit charge and discharge power in KW by $P_{b.ch}^{min}$, $P_{b.dis}^{min}$, and the maximum limit charge and discharge power in KW by P_b^{max}, P_b^{min}, and $U_{b.ch}^{t}$, $U_{b.dis}^{t}$. The following is anexchange ofn for the exchanging ESS power in KWh:

$$P_b^t = P_{b.dis}^{t} - P_{b.ch}^{t} \tag{38}$$

When the ESS is purchasing a micro grid, the P_b^t is (+); when the battery is charging, it is (-). Depended on battery charge discharge principle ω_b in $/KWh, the cost of ESS at operating battery C_b^t in $ is:

$$C_b^t = P_b^t * \omega_b \tag{39}$$

2.13 Heat storage system model

When heat power is available, it is stored in heat storage system (HSS) for later use in the event that a heat source is unavailable. The state of charge for battery SOC_h^t in KWh can be expressed by [40]:

$$SOC_{hs}^{t} = SOC_{hs}^{t-1} - \frac{H_{hs.dis}^{t}}{\eta_{hs.dis}} + H_{hs.ch}^{t}\,\eta_{hs.ch} \tag{40}$$

The charging and discharging power HSS in KWh is represented by $H_{hs.ch}^{t}, H_{hs.dis}^{t}$, while the charging and discharging efficiency is represented by $\eta_{hs.ch}, \eta_{hs.dis}$. The HSS's constraint capacity may be stated as follows:

$$H_{hs}^{min} \le H_{hs}^{t} \le H_{hs}^{max} \tag{41}$$

$$H_{hs.ch}^{min} U_{hs.ch}^{t} \le H_{hs.ch}^{t} \le H_{hs.ch}^{max} U_{hs.ch}^{t} \tag{42}$$

$$H_{hs.dis}^{min} U_{hs.ch}^{t} \le H_{hs.dis}^{t} \le H_{hs.dis}^{max} U_{hs.dis}^{t} \tag{43}$$

$$U_{hs.dis}^{t} + U_{hs.ch}^{t} \le 1 \tag{44}$$

The minimum limit charge and discharge power of the battery is represented by $H_{hs.ch}^{min}$, $H_{hs.dis}^{min}$ in KW, the maximum limit charge and discharge power of the HSS in KW is represented by $H_{hs.ch}^{max}$, $H_{hs.dis}^{max}$, and the on/off states of charge and discharge are represented by $U_{hs.ch}^{t}$, $U_{hs.dis}^{t}$. The following is an expression for the exchange HSS power in KWh:

$$H_{hs}^{t} = H_{hs.dis}^{t} - H_{hs.ch}^{t} \quad (45)$$

In a discharge condition, when the HSS purchases power from the microgrid, the H_{hs}^{t} is (+); in a charging state, when the HSS consumption is (–). Depended on HSS charge discharge prince ω_{hs} in \$/KWh, the cost of HSS at operation battery C_{hs}^{t} in \$ is:

$$C_{hs}^{t} = H_{hs}^{t} * \omega_{hs} \quad (46)$$

2.14 Power and utility grid interaction

Because it shares energy with the gird based on demand response, exports power when there is an excess of electrical power production due to the availability of RE sources, and imports power when electrical prices are low and it is cost-effective to import from the gird rather than operating production units or when there is a deficit in meeting demand, the CCHP-MG was connected to the gird to increase its reliability and stability [41]. With the utility grid, the trading power P_{UG}^{t} in KWh may be written as follows:

$$P_{UG}^{t} = P_{import}^{t} - P_{export}^{t} \quad (47)$$

where, P_{import}^{t} is importing electricity from the grid in (KWh) and P_{export}^{t} is export electricity to grid in KWh, the P_{UG}^{t} t (+) at import purchasing state, and (−) at export selling. The power trading cost $C_{e.UG}^{t}$ in \$ deponed on electrical prince $\omega_{elect.}^{t}$ in $(\frac{\$}{KWh})$ is:

$$C_{e.UG}^{t} = P_{UG}^{t} * \omega_{elect.}^{t} \quad (48)$$

The constraint capacity of the interacting power it can be expressed by:

$$P_{import}^{min}\ U_{e.import}^{t} \le P_{import}^{t} \le P_{import}^{mas}\ U_{e.import}^{t} \quad (49)$$

$$P_{export}^{min}\ U_{e.export}^{t} \le P_{export}^{t} \le P_{export}^{mas}\ U_{e.export}^{t} \quad (50)$$

$$U_{e.import}^{t} + U_{e.export}^{t} \le 1 \quad (51)$$

where, $U_{e.import}^{t}$ electrical import on/off state and P_{import}^{min}, P_{import}^{max} limit power can be imported. Additionally, $U_{e.export}^{t}$ electrical export on/off state and P_{export}^{min}, P_{export}^{max} limit power can be exported.

2.15 Heat power with upstream grid model

Because it shares heat energy with the gird based on demand response, exports heat power when there is a surplus, and imports heat when heat prices are low and it is cost-effective to import from the gird rather than operating production units or when there is a deficit in meeting demand, the CCHP-MG was connected to the District Heating Network (DHN) or the heat upstream gird in order to increase the reliability of the gird [31]. With the utility grid, the trading power H_{UG}^{t} in KWh may be written as:

$$H_{UG}^{t} = H_{import}^{t} - H_{export}^{t} \quad (52)$$

where, H_{import}^{t} is using grid-imported thermal power in KWh and H_{export}^{t} is the grid's source of thermal electrical power in KWh, the H_{UG}^{t} t (+) at import purchasing state, and (−) at export selling. The power heat trading cost $C_{h.UG}^{t}$ in \$ deponed on electrical prince $\omega_{heat.}^{t}$ in $(\frac{\$}{KWh})$ is:

$$C_{h.UG}^{t} = H_{UG}^{t} * \omega_{heat.}^{t} \quad (53)$$

The constraint capacity of the interacting heat power can be expressed by:

$$H_{import}^{min}\ U_{h.import}^{t} \le H_{import}^{t} \le H_{import}^{mas}\ U_{h.import}^{t} \quad (54)$$

$$H_{export}^{min}\ U_{h.export}^{t} \le H_{export}^{t} \le H_{export}^{mas}\ U_{h.export}^{t} \quad (55)$$

$$U_{h.import}^{t} + U_{h.export}^{t} \le 1 \quad (56)$$

where, H_{import}^{min}, H_{import}^{mas} limit power can be imported and $U_{e.import}^{t}$ heat import on/ off state. And where H_{export}^{min}, H_{export}^{mas} limit power can be exported and $U_{h.export}^{t}$ heat export on/off state.

2.16 Model of emission costs

Greenhouse gases (GHGs) such as carbon dioxide (CO_2), sulfur dioxide (SO_2), nitrogen oxides (Nox), and particulate matter (PM) are released during the energy production process, with the exception of RE sources. It is crucial to minimize these emissions. According to the monetary notion of cost constraint, the released gases are therefore seen as a cost in the cost objective function. The expression for the total emission cost $C_{Emi.}^{t}$ in \$ is as follows [42]:

$$C_{Emi.}^{t} = \sum_{1}^{i} \sum_{1}^{j} P_{i}^{t}\ C_{j}\ E_{i,j} \quad (57)$$

where, P_{i}^{t} (KWh) is the power product can emotion GHGs of i^{th} in this research DG, MT, and FC. The C_j in $(\frac{\$}{Kg})$ this is expense of emission prince of j^{th} GHG in this research is CO_2, So_2, No_x, and PM. The $E_{i,j}$ in $(\frac{Kg}{KWh})$ this is the amount of can emission j^{th} where product power for each i^{th}.

2.17 Power balance constraint model

This limitation must be met in order to guarantee that electrical power production meets the necessary electrical demand loads for each time:

$$\begin{aligned} P_{MT}^{t} + P_{FC}^{t} + P_{DG}^{t} + P_{PV}^{t} + P_{WT}^{t} + P_{b.dis}^{t} + P_{import}^{t} \\ = P_{export}^{t} + P_{b.ch}^{t} + P_{ce}^{t} + P_{EH}^{t} \\ + L_{elctr.}^{t} \end{aligned} \quad (58)$$

where, L_{elctr}^{t} is a load that requires electrical power in KWh.

To ensure that heat power is supplied that satisfies the required heat demand loads for each period, this restriction must be fulfilled:

$$\begin{aligned} H_{MT}^{t} + H_{GB}^{t} + P_{SAH}^{t} + H_{EH}^{t} + H_{b.dis}^{t} + H_{import}^{t} = \\ H_{export}^{t} + H_{b.ch}^{t} + H_{ca}^{t} + L_{heat.}^{t} \end{aligned} \quad (59)$$

where, L_{heat}^{t} is heat power demand load in KWh.

To ensure that cool electricity is supplied that satisfies the required cool demand loads for each period, this restriction

must be observed:

$$P_{ce}^{t} + H_{ca}^{t} = P_{c}^{t} + L_{cool.}^{t} \quad (60)$$

where, $L_{cool.}^{t}$ is cool power demand load in KWh.

2.18 Objective function cost model

In order to obtain the minimal cost function CF in $, this study changed its multi-objective goal to a single aim by considering emission cost as a monetary notion [43].

$$CF = \sum_{t=1}^{24} [\, C_{MT}^{t} + {SUC_{MT}}^{t} + {SDC_{MT}}^{t} + C_{om.MT}^{t} + {C_{FC}}^{t} + {SUC_{FC}}^{t} + {SDC_{FC}}^{t} + C_{om.FC}^{t} + {C_{DG}}^{t} + {SUC_{DG}}^{t} + SDU_{DG}^{t} + C_{om.DG}^{t} + {C_{GB}}^{t} + C_{om.GB}^{t} + C_{b}^{t} + C_{hs}^{t} + C_{e.UG}^{t} + C_{h.UG}^{t} + C_{Emi.}^{t}] \quad (61)$$

3. CASE STUDY

Figure 1 illustrates the system topology used in this study. It includes GB, EH, and a heat recovery system from MT to cover thermal loads and FC, MT, and DG to cover electrical loads. In addition to the renewable sources listed in Table 1, which include WT and PV for electrical loads and SAH for thermal loads, PV is used in this investigation. Four cases were tested: one without SAH, one with SAH of type Case 1, one with SAH of type Case 2, one with SAH of type Case 3, and one with SAH of type Case 4. Each scenario had a number of 100. Systems for electrical and thermal storage and cooling were also employed (Table 2). The emissions were listed in Table 3. Table 1 hourly loads, prices, and renewable generation [31, 42]. Data for the system are shown in Tables 4–7.

Table 2. Energy and heat storage system parameter

Type	P_{ch}^{max} KW	P_{ch}^{min} KW	P_{dis}^{max} KW	P_{dis}^{min} KW	P^{max} KW	P^{min} KW	η_{ch}	η_{dis}	ω ($\frac{\$}{KWh}$)
Energy Storage System (ESS)	90	1	90	1	300	90	0.9	0.9	0.06
Heat Storage System (HSS)	90	1	90	1	300	90	0.9	0.9	0.003

Table 3. Emission parameters

Source	E_{CO2} ($\frac{Kg}{KWh}$)	E_{NOx} ($\frac{Kg}{KWh}$)	E_{SO2} ($\frac{Kg}{KWh}$)	E_{PM} ($\frac{Kg}{KWh}$)
DG	0.848	0.0013	0.00125	0.00036
FC	0.489	0.00001	0.000003	0.000001
MT	0.725	0.0002	0.000004	0.000041
C_j($\frac{\$}{Kg}$)	**0.02**	**5**	**6**	**25**

Table 4. Properties of absorber and electric chillers (EC)

Elect	P_i^{min} KW	P_i^{max} KW	η_i	$POC_{e,a}$ $/KWh	UR_i KW	DR_i KW
Cce	0	100	0.85	4	150	150
Cca	0	200	0.85	0.8	160	160

Table 5. PV parameter

	PV Area m^2	No. PV	η_{PV}
PV	2.374	150	24

Table 6. Heat recovery parameter

	η_l	η_{HR}
HR	0.2	0.75

Table 7. Natural gas parameters

LCV ($\frac{KWh}{m^3}$)	β_g ($\frac{\$}{m^3}$)
9.78	0.4

4. THE SOLUTION OF THE OPTIMAL PROBLEM

A combined-objective UCIMIQP is the formulation of the suggested EMS. A single function that can be solved directly in a single step develops from this integrated objective optimization function [44]. Software called the General Algebraic Modeling System (GAMS) is used to construct and describe the suggested optimization problem [45]. Gams is an extremely mathematical modeling system used to solve optimization challenges. To solve the suggested CCHP optimization issue, the NLP solver is employed. The procedure used to define and resolve the suggested optimization issue is illustrated in the flowchart, as shown in Figure 4.

First, the economic operation function serves as the foundation for the formulation of each CCHP component. Furthermore, the operation-related constraints are developed and modeled in the way described in the preceding section. Additionally, the combined goal function is designed to reduce the cost of operation and emissions. At last, the entire issue is resolved, and the results are shown. Absent optimization, the system in the suggested CCHP doesn't work. This is due to the interaction between the heating, cooling, and electric systems, where energy is transformed into different forms to ensure optimal system performance. Furthermore, the pricing structure governs energy trading with the main grid, and it is

challenging to predict the timing and volume of energy exchanges with the utility grid.

The suggested CCHP system operates in a cheap and environmentally friendly approach because of the interaction between the electric, heating, and cooling systems. As a result, the objective function's formulation takes these systems' interactions into account.

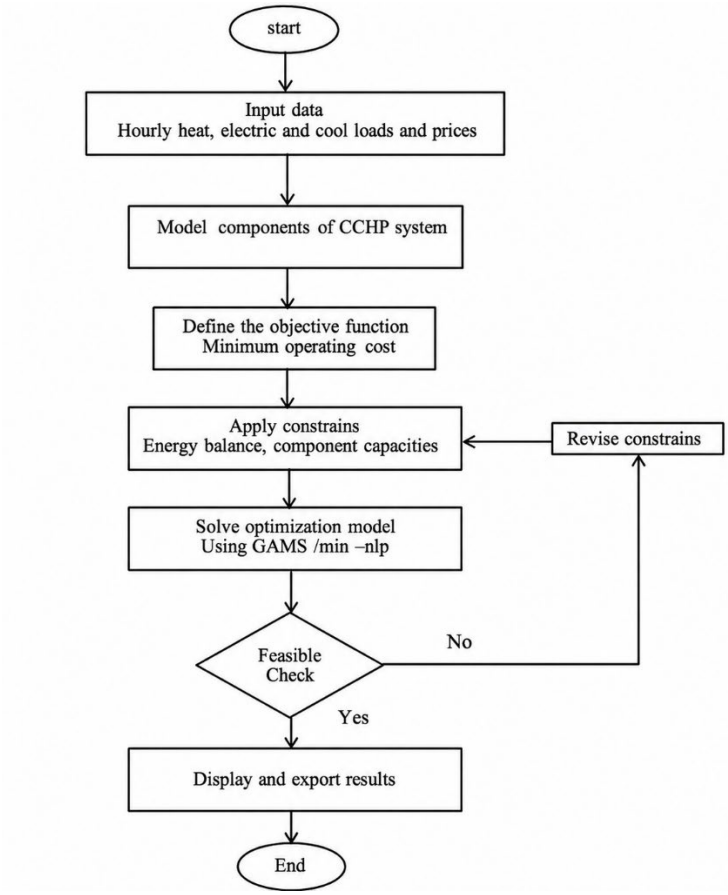

Figure 4. Flow chat of model and solution the proposed system

5. RESULTS AND DISCUSSION

In order to attain the least optimization cost, the suggested grid has been solved by MIQP on the UC technique in GAMS. The output heat power was experimentally measured in January in Baghdad for 4 situations using the SAH model from SAH, as shown in Figure 5, scenario 1, without SAH in this study, which examined five scenarios with SAH. scenario 1 had the highest total cost for the day at $1132.025, followed by scenario 2 in case 1 with $1104.582, scenario 3 with $1096.22, scenario 4 in case 3 with $1190.25, and scenario 5 with $1074.482. The cost for all cases for each time is shown in Table 8 and explained in Figure 6.

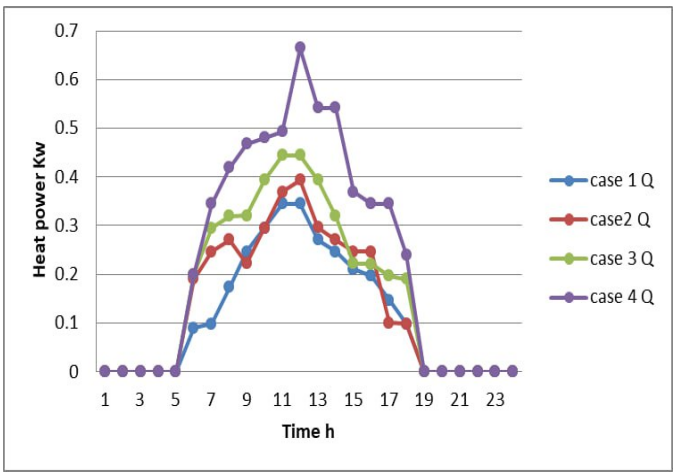

Figure 5. Optimal output heat generated by solar air heater (SAH)

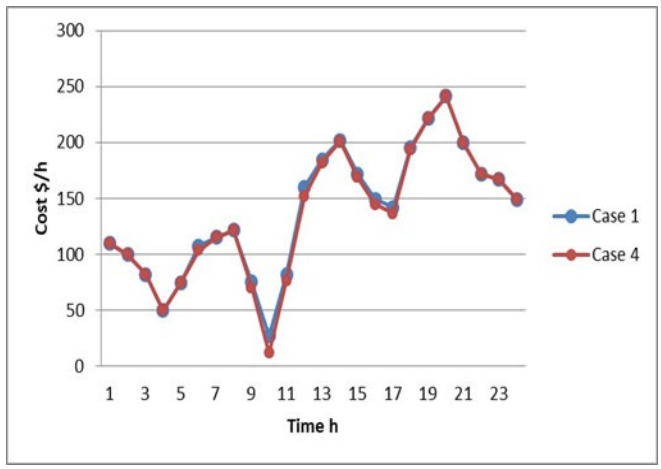

Figure 6. Total cost hourly for scenario 1 and 5

Table 8. Cost per time of combined cooling, heating, and power (CCHP) for scenarios 1 and 5 in $

	Scenario 1			Scenario 5		
Time (h)	Electrical Cost	Heat Cost	Cool Cost	Electrical Cost	Heat Cost	Cool Cost
t1	34.52958	-15.543	87.3	34.52958	-15.543	87.3
t2	35.21497	0.040812	61.11	35.21497	0.040812	61.11
t3	34.37438	0.81762	43.65	34.37438	0.81762	43.65
t4	34.11823	-13.9445	26.19	34.11823	-13.9445	26.19
t5	26.70413	10.11707	34.92	26.70413	10.11707	34.92
t6	34.97316	9.928068	59.36	31.71694	9.882529	59.36
t7	23.55238	9.34436	78.57	23.55238	9.244726	78.57
t8	1.285958	9.838046	104.8	1.285958	9.853949	104.8
t9	-34.2182	6.772332	96.03	-34.2182	1.380972	96.03
t10	-54.3221	-3.55043	78.57	-54.3221	-18.9027	78.57
t11	-16.0709	1.694568	89.57	-16.0709	-3.80731	89.57
t12	37.45195	3.891501	113.5	37.45195	-4.51038	113.5
t13	18.98904	9.349068	148.4	16.278	9.429544	148.4
t14	55.48424	9.628068	131	53.15781	9.628068	131
t15	53.48127	3.870372	109.1	53.48127	0.947892	109.1
t16	53.33366	-5.96317	97.77	53.33366	-10.3102	97.77
t17	49.55651	-3.86826	92.56	49.55651	-9.61826	92.56
t18	50.82747	9.997828	131	49.26135	9.97849	131
t19	56.1995	10.03809	150.2	56.1995	10.03809	150.2
t20	68.22471	10.20817	157.14	68.22471	10.20817	157.14
t21	51.71351	10.74188	131	51.71351	10.74188	131
t22	50.17223	10.63412	104.8	50.17223	10.63412	104.8
t23	49.44578	10.14745	101.3	49.44578	10.14745	101.3
t24	43.27258	9.050088	91.7	43.27258	9.050088	91.7

It was observed that by using the SAH collector for scenario 5, the cost was reduced by 27.8%, this means that the heat added to the micro grids has led to this cost reduction. Where a profit of approximately $59 per day.

Table 9 shows the hourly thermal performance of four different setups of SAHs. The findings show how system design improves thermal efficiency and show distinct patterns in the behavior of heat generation during a normal 24-hour cycle.

Table 9. Output heat generation from solar air heater (SAH) cases in KW

Time	SAH 1	SAH 2	SAH 3	SAH 4
t1	0	0	0	0
t2	0	0	0	0
t3	0	0	0	0
t4	0	0	0	0
t5	0	0	0	0
t6	0.09	0.19	0.2	0.2
t7	0.098	0.246	0.295	0.345
t8	0.173	0.271	0.32	0.4189
t9	0.246	0.2218	0.321	0.468
t10	0.295	0.295	0.394	0.481
t11	0.345	0.369	0.444	0.493
t12	0.345	0.394	0.445	0.665
t13	0.271	0.296	0.394	0.542
t14	0.246	0.271	0.32	0.542
t15	0.21	0.246	0.222	0.369
t16	0.197	0.246	0.221	0.345
t17	0.147	0.1	0.197	0.345
t18	0.098	0.098	0.19	0.24
t19	0	0	0	0
t20	0	0	0	0
t21	0	0	0	0
t22	0	0	0	0
t23	0	0	0	0
t24	0	0	0	0

Figure 7 presents the CCHP system's hourly heat, electric, and cooling load needs over a 24-hour period. The CCHP components, about 574 kW for heat, 421 kW for electricity, and 157 kW for cooling, are designed for peak usage.

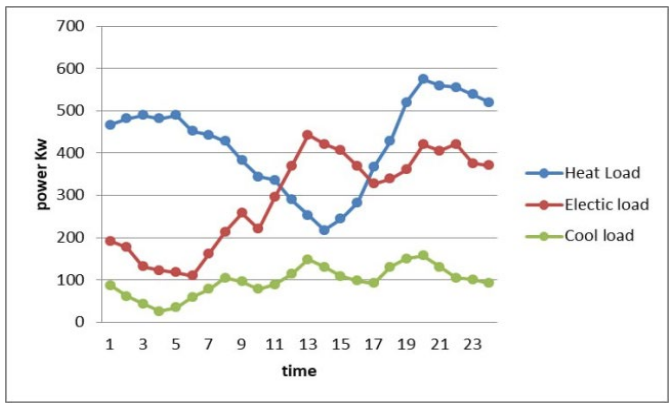

Figure 7. Power load demand

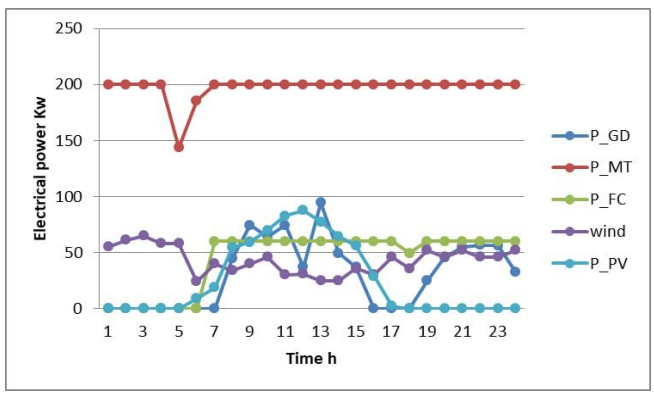

Figure 8. Optimal electrical power schedule with electrical load scenario 1

The generation of electrical energy sources for scenarios (1

and 5) is described in Figures 8 and 9, which are similar. Due to its high running costs and lack of economic viability in comparison to the inexpensive and fully capable production of electrical energy from MT, DG is always in the off state. In addition to the existence of FC, which is switched on at t7, the remaining energy is provided by renewable sources RE, which include WT and PV, as the work of the MT lengthens the time to compensate for the deficiency that occurs at the peak of pregnancy.

Figures 10 and 11 show the meeting of electrical needs from the grid, where it is less expensive and more cost-effective than using DG. Electricity is exported to the grid between t7 and t13, where it is operated by RE sources. When MT is operating at full capacity, power prices are high, and selling the generated electricity to the grid is lucrative.

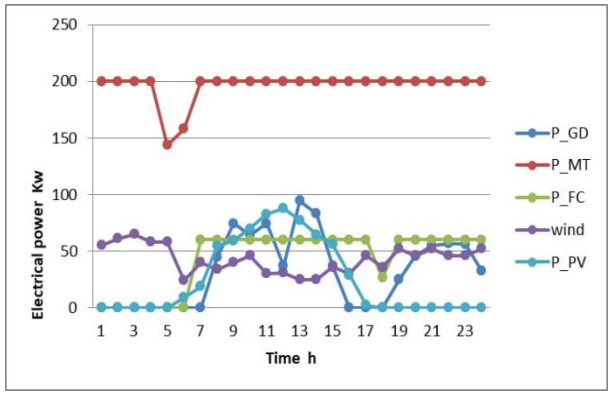

Figure 9. Optimal electrical power schedule with electrical load scenario 5

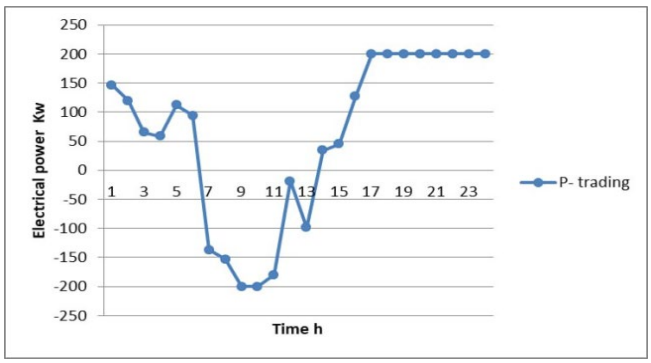

Figure 10. Exchange of electrical power with the grid scenario 1

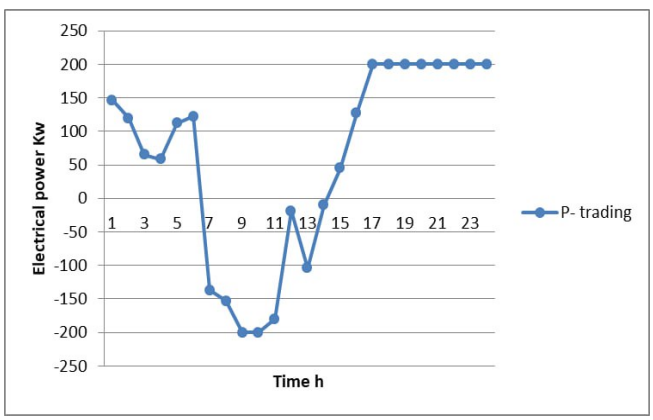

Figure 11. Exchange of electrical power with the grid scenario 5

Figure 12 explains that the battery rests at its maximum capacity for the majority of the time in scenarios 1 and 5, and its charge is discharged to the MG during t9–t13 to help cover the loads. The batteries are charged during t13, when the WT and PV are producing at their highest levels, to store this energy and release it in the morning.

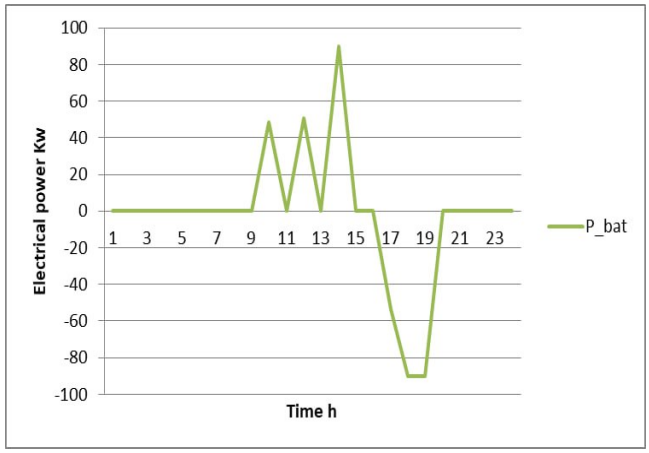

Figure 12. Optimal power schedule of Energy Storage System (ESS) scenario 1 and 5

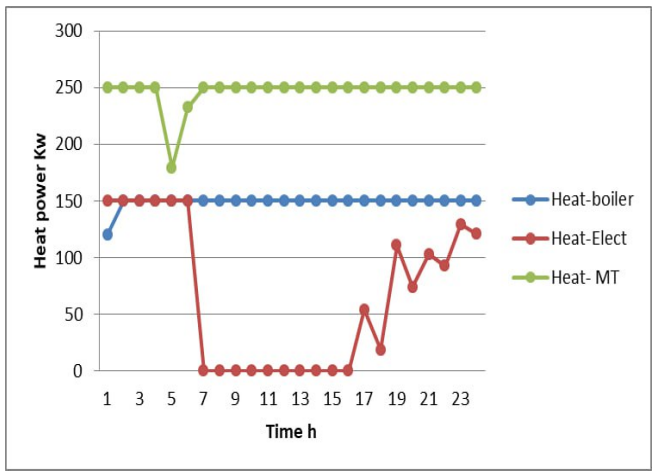

Figure 13. Optimal heat power schedule with heat load scenario 1

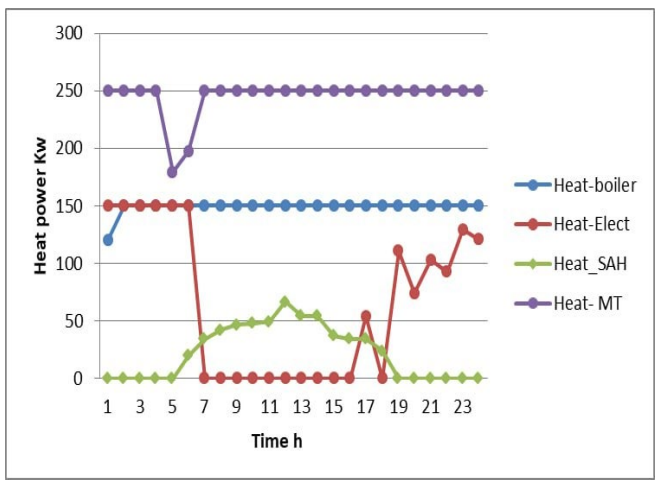

Figure 14. Optimal heat power schedule with heat load scenario 5

Figures 13 and 14 show that the majority of the thermal loads are met by recovering the waste heat from the MT, with the remainder being met by the GB. The EH will attempt to meet the remaining loads for scenario 1 during periods of peak heat demand, which are t1–t7 and t16–t24. Instead of covering the loads and lowering the output of the remaining heat sources, it is more cost-effective to export and sell this heat differential to the network when adding SAH in scenario 5, which contributes from t5 to t19. By storing heat during periods of plenty till periods when heat is scarce, the thermal battery TEE balances the production and demand for heat in both situations.

Figures 15 and 16 show that the EC usually provides cooling during the day because the price of gas is high, as mentioned previously, and also the number of PVs is large, which makes the cost of electricity for cooling less than heating, so the absorber chiller only works at the time t13, t14 when the price of electricity is at its highest.

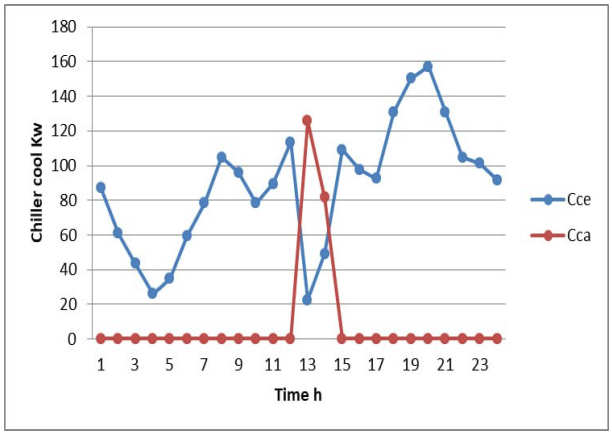

Figure 15. Cool power exchange with grid scenario 1

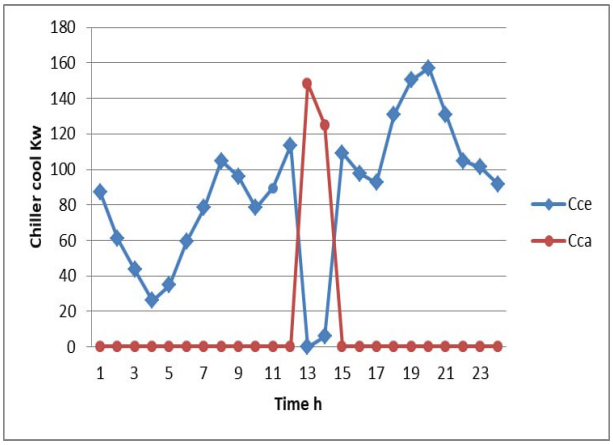

Figure 16. Cool power exchange with grid scenario 5

When studying the microgrid system, it is necessary to identify the emissions from electrical and thermal devices in order to limit these and reduce their cost. Figure 17 shows that it is evident from the comparison that Case 4 outperforms Case 1 in terms of emissions. Even while emissions in the early morning and late evening don't change much, the decreases in the daytime validate that higher renewable penetration with SAH has successfully reduced emissions.

Thermodynamics provides an explanation for the notable 27.8% cost decrease attained by using solar heating. Conventional heat generating machines utilize less fuel because solar air heating offers a direct supply of low-grade thermal energy. As a result, the CCHP system uses less fuel overall, which lowers operating expenses and emissions.

Solar heating immediately replaces fuel-based thermal generating and lowers carbon emissions, providing substantial environmental benefits in addition to economic ones. Solar heating reduces fuel consumption for thermal loads, leading to a more direct emission reduction than PV and wind systems, which primarily balance electricity demand. Solar heating has a greater overall effect on emission reduction since there are no conversion losses, demonstrating its usefulness as an additional renewable technology in CCHP systems.

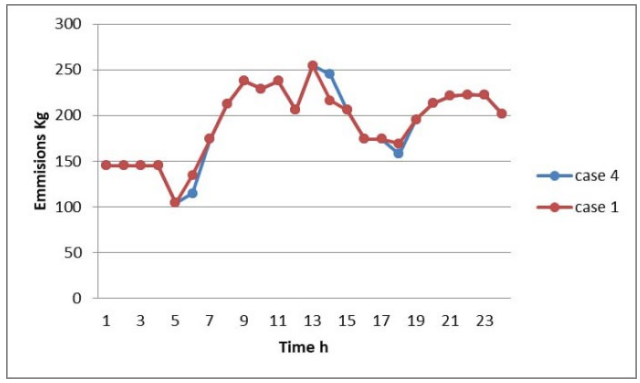

Figure 17. Emissions in Kg with grid scenario 1 and 5

6. CONCLUSION

This study presents an experimental investigation of an innovative design of SAH are developed experimentally tested. These types of SAHs are integrated with the proposed CCHP system in one novel approach. The optimization problem is formulated as MOMINL with consideration of the UC strategy in both electric and heat systems to reduce both the operating and emission costs. The emission level of GHGs is converted into monetary form, allowing the problem to be solved directly in a single step. According to the findings, adding solar heating to the CCHP system lowers carbon emissions while cutting overall running costs from $1132 to $1074 and a 27.8% cost savings. Besides, the charging and discharging operation of the storage devices minimizes the operating and emission costs. The proposed optimization framework provides a practical tool for designing and operating low-carbon microgrids, enabling energy planners to reduce both costs and emissions in real-world CCHP applications.

This study has certain limitations despite the encouraging outcomes. The suggested model is predicated on a number of energy consumption and system functioning assumptions that could not hold true in the actual world. Additionally, weather information and solar availability, which might change depending on the location and season, have an impact on how well solar heating works. In order to confirm the applicability of the suggested approach in real-world microgrid deployments, further work will concentrate on integrating uncertainty analysis with real-time operational data.

ACKNOWLEDGMENT

The authors would like to express their sincere appreciation to the University of Technology for its valuable.

REFERENCES

[1] Kang, L., Sun, D., Zhao, W., Wang, W., Wu, X., Zhang, X., Yang, Y., Wang, Y. (2024). Research on optimization method of CCHP system coupled with renewable energy. Science and Technology for Energy Transition, 79: 70. https://doi.org/10.2516/stet/2024069

[2] Wang, L., Lin, J., Dong, H., Wang, Y., Zeng, M. (2023). Demand response comprehensive incentive mechanism-based multi-time scale optimization scheduling for park integrated energy system. Energy, 270: 126893. https://doi.org/10.1016/j.energy.2023.126893

[3] Xu, B., Wang, J., Guo, M., Lu, J., Li, G., Han, L. (2021). A hybrid demand response mechanism based on real-time incentive and real-time pricing. Energy, 231: 120940. https://doi.org/10.1016/j.energy.2021.120940

[4] Li, G., Zhang, R., Jiang, T., Chen, H., Bai, L., Cui, H., Li, X. (2017). Optimal dispatch strategy for integrated energy systems with CCHP and wind power. Applied Energy, 192: 408-419. https://doi.org/10.1016/j.apenergy.2016.08.139

[5] Assareh, E., Dejdar, A., Ershadi, A., Jafarian, M., Mansouri, M., roshani, A.S., Azish, E., Saedpanah, E., Lee, M. (2023). Techno-economic analysis of combined cooling, heating and power system integrated with renewable energy and energy storage. Energy and Buildings, 278: 112618. https://doi.org/10.1016/j.enbuild.2022.112618

[6] Maraver, D., Sin, A., Royo, J., Sebastian, F. (2013). Assessment of CCHP systems based on biomass combustion for small-scale applications through a review of the technology and analysis of energy efficiency parameters. Applied Energy, 102: 1303-1313. https://doi.org/10.1016/j.apenergy.2012.07.012

[7] Wang, J., You, S., Zong, Y., Traeholt, C., Zhou, Y., Mu, S. (2019). Optimal dispatch of combined heat and power plant in integrated energy system: A state of the art review and case study of Copenhagen. Energy Procedia, 158: 2794-2799. https://doi.org/10.1016/j.egypro.2019.02.040

[8] Tiwari, V., Dubey, H.M., Pandit, M., Salkuti, S.R. (2022). CHP-based economic emission dispatch of microgrid using Harris Hawks optimization. Fluids, 7(7): 248. https://doi.org/10.3390/fluids7070248

[9] Ahn, H., Miller, W., Sheaffer, P., Tutterow, V., Rapp, V. (2021). Opportunities for installed combined heat and power (CHP) to increase grid flexibility in the U.S. Energy Policy, 157: 112485. https://doi.org/10.1016/j.enpol.2021.112485

[10] Gu, M.Z.W., Wang, X.Y. (2010). Microgrid economic optimal operation of the combined heat and power system with renewable energy. In IEEE PES General Meeting, Minneapolis, MN, USA, pp. 1-6. https://doi.org/10.1109/PES.2010.5590140

[11] Ma, Z., Bloch-Hansen, K., Buck, J.W., Hansen, A.K., Henriksen, L.J., Thielsen, C.F., Santos, A.Q., Jorgensen, B.N. (2018). Peer-to-peer trading solution for microgrids in Kenya. In 018 IEEE PES/IAS PowerAfrica, Cape Town, South Africa, pp. 1-425. https://doi.org/10.1109/PowerAfrica.2018.8520980

[12] Parisio, A., Rikos, E., Glielmo, L. (2016). Stochastic model predictive control for economic/environmental operation management of microgrids: An experimental case study. Journal of Process Control, 43: 24-37. https://doi.org/10.1016/j.jprocont.2016.04.008

[13] Smaisim, G.F., Abed, A.M., Hadrawi, S.K., Majdi, H.S., Shamel, A. (2023). Modelling and optimization of combined heat and power system in microgrid based on renewable energy. Clean Energy, 7(4): 735-746. https://doi.org/10.1093/ce/zkad012

[14] Hu, P., Cao, C., Dai, S. (2020). Optimal dispatch of combined heat and power units based on particle swarm optimization with genetic algorithm. AIP Advances, 10(4): 045008. https://doi.org/10.1063/1.5145074

[15] Alam, M.S., Arefifar, S.A. (2019). Energy management in power distribution systems: Review, classification, limitations and challenges. IEEE Access, 7: 92979-93001. https://doi.org/10.1109/ACCESS.2019.2927303

[16] Houwing, M., Negenborn, R.R., De Schutter, B. (2011). Demand response with micro-CHP systems. Proceedings of the IEEE, 99(1): 200-213. https://doi.org/10.1109/JPROC.2010.2053831

[17] Abdulmunem, A.R., Jabal, M.H., Samin, P.M., Rahman, H.A., Hussien, H.A. (2019). Analysis of energy and exergy for the flat plate solar air collector with longitudinal fins embedded in paraffin wax located in Baghdad center. International Journal of Heat and Technology, 37(4): 1180-1186. https://doi.org/10.18280/ijht.370428

[18] Yuan, R., Ye, J., Lei, J., Li, T. (2016). Integrated combined heat and power system dispatch considering electrical and thermal energy storage. Energies, 9(6): 474. https://doi.org/10.3390/en9060474

[19] Erixno, O., Rahim, N.A., Ramadhani, F., Adzman, N.N. (2022). Energy management of renewable energy-based combined heat and power systems: A review. Sustainable Energy Technologies and Assessments, 51: 101944. https://doi.org/10.1016/J.SETA.2021.101944

[20] Salman, C.A., Li, H., Li, P., Yan, J. (2021). Improve the flexibility provided by combined heat and power plants (CHPs) – A review of potential technologies. e-Prime - Advances in Electrical Engineering, Electronics and Energy, 1: 100023. https://doi.org/10.1016/j.prime.2021.100023

[21] Dobre, C., Costin, M., Constantin, M. (2024). A review of available solutions for implementation of small–medium combined heat and power (CHP) systems. Inventions, 9(4): 82. https://doi.org/10.3390/inventions9040082

[22] Jafari, E., Soleymani, S., Mozafari, B., Amraee, T. (2018). Optimal operation of a micro-grid containing energy resources and demand response program. International Journal of Environmental Science and Technology, 15(10): 2169-2182. https://doi.org/10.1007/s13762-017-1525-6

[23] Ma, D., Zhang, L., Sun, B. (2021). An interval scheduling method for the CCHP system containing renewable energy sources based on model predictive control. Energy, 236: 121418. https://doi.org/10.1016/j.energy.2021.121418

[24] Jia, J.D., Chen, H.W., Liu, H.T., Ai, T.C., Li, H.Q. (2021). Thermodynamic performance analyses for CCHP system coupled with organic Rankine cycle and solar thermal utilization under a novel operation strategy. Energy Conversion and Management, 239: 114212. https://doi.org/10.1016/j.enconman.2021.114212

[25] Soheyli, S., Mayam, M.H.S., Mehrjoo, M. (2016). Modeling a novel CCHP system including solar and wind

renewable energy resources and sizing by a CC-MOPSO algorithm. Applied Energy, 184: 375-395. https://doi.org/10.1016/j.apenergy.2016.09.110
[26] Ren, F., Wei, Z., Zhai, X. (2021). Multi-objective optimization and evaluation of hybrid CCHP systems for different building types. Energy, 215: 119096. https://doi.org/10.1016/j.energy.2020.119096
[27] Ge, Y., Han, J.T., Ma, Q.Z., Feng, J.H. (2022). Optimal configuration and operation analysis of solar-assisted natural gas distributed energy system with energy storage. Energy, 246: 123429. https://doi.org/10.1016/j.energy.2022.123429
[28] Stanek, W.W., Gazda, W., Kostowski, W. (2015). Thermoecological assessment of CCHP (combined cold-heat-and-power) plant supported with renewable energy. Energy, 92: 279-289. https://doi.org/10.1016/j.energy.2015.02.005
[29] Ruan, Y.J., Liang, Z.Y., Qian, F.Y., Meng, H., Gao, Y. (2023). Operation strategy optimization of combined cooling, heating, and power systems with energy storage and renewable energy based on deep reinforcement learning. Journal of Building Engineering, 65: 105682. https://doi.org/10.1016/j.jobe.2022.105682
[30] Song, A., Zhu, J., Zhang, P. (2019). Experimental research on solar and geothermal energy coupling power generation system. Energy Procedia, 158: 5982-5987. https://doi.org/10.1016/j.egypro.2019.01.522
[31] Al-Saadi, M.K., Luk, P. (2022). Profit-based online optimal planning of low emission multi-energy distribution system. Journal of Engineering Science and Technology, 17(2): 1287-1305.
[32] Tan, B., Chen, H. (2019). Stochastic multi-objective optimized dispatch of combined cooling, heating, and power microgrids based on hybrid evolutionary optimization algorithm. IEEE Access, 7: 176218-176232. https://doi.org/10.1109/ACCESS.2019.2955515
[33] Geng, S., Wu, G., Tan, C., Niu, D., Guo, X. (2021). Multi-objective optimization of a microgrid considering the uncertainty of supply and demand. Sustainability, 13(3): 1320. https://doi.org/10.3390/su13031320
[34] Liu, H., Ji, Y., Zhuang, H., Wu, H. (2015). Multi-objective dynamic economic dispatch of microgrid systems including vehicle-to-grid. Energies, 8(5): 4476-4495. https://doi.org/10.3390/en8054476
[35] Li, Y., Zou, Y., Tan, Y., Cao, Y., Liu, X., Shahidehpour, M., Tian, S., Bu, F. (2018). Optimal stochastic operation of integrated low-carbon electric power, natural gas, and heat delivery system. IEEE Transactions on Sustainable Energy, 9(1): 273-283. https://doi.org/10.1109/TSTE.2017.2728098
[36] Ghafoor, M.S.A., Al-Saadi, M.K., Jaddoa, A.A. (2025). Comparative study on the performance of a solar air heater using aluminum soda cans with different arrangements. Frontiers in Heat and Mass Transfer, 23(3): 975-990. https://doi.org/10.32604/fhmt.2025.064025
[37] Alaskaree, E.H., Breesam, Y.F. (2024). The impact of electronic control systems on improving the performance of the solar heater. Engineering and Technology Journal, 42(7): 869-884. https://doi.org/10.30684/etj.2024.145174.1652
[38] Habeeb, G.A., Jaddoa, A.A., Alkhasraji, J.M.D. (2025). A numerical study of the solar air heater performance using artificial spherical obstacles. International Journal of Heat and Technology, 43(2): 703-720. https://doi.org/10.18280/ijht.430230
[39] Shafi, S.T.A., Al-Saadi, M.K., Jaddoa, A.A. (2025). Optimizing solar air heater performance using perforated V-shaped barriers with varied geometric designs. Frontiers in Heat and Mass Transfer, 23(2): 703-719. https://doi.org/10.32604/fhmt.2025.063118
[40] Zhong, Y., Xie, D., Zhai, S., Sun, Y. (2018). Day-ahead hierarchical steady state optimal operation for integrated energy system based on energy hub. Energies, 11(10): 2765. https://doi.org/10.3390/en11102765
[41] Rezaee Jordehi, A. (2021). Economic dispatch in grid-connected and heat network-connected CHP microgrids with storage systems and responsive loads considering reliability and uncertainties. Sustainable Cities and Society, 73: 103101. https://doi.org/10.1016/j.scs.2021.103101
[42] Bilal, G.A., Al-Saadi, M.K., Al-Sultany, G.A., Al-Maliki, W.A.K. (2025). Optimal operation of CCHP smart distribution grid with integration of renewable energy. Applied Sciences, 15(3): 1407. https://doi.org/10.3390/app15031407
[43] Jabber, K.M., Al-Saadi, M.K., Jaddoa, A.A. (2023). Economic operation of low voltage smart micro-grid with integration of renewable energy. Engineering and Technology Journal, 40(7): 951-958. https://doi.org/10.30684/etj.2023.142456.1263
[44] Hamedi, H. (2013). Solving the combined economic load and emission dispatch problems using new heuristic algorithm. International Journal of Electrical Power and Energy Systems, 46: 10-16. https://doi.org/10.1016/j.ijepes.2012.09.021
[45] Adetona, S.O., Adetola, M.Y., Okafor, F.N., Ubakanwa, G. (2024). Impact of the UPFC on the optimal transmission switching for cutting down market power cost. Engineering and Technology Journal, 42(2): 312-326. https://doi.org/10.30684/etj.2024.144807.1645

NOMENCLATURE

P^{max}	Maximum power can be generated (KW)
P^{min}	Minimum power can be generated (KW)
Sc	Price Startup cost ($)
Sd	Price Shutdown cost ($)
UR_i	Ramp up power (KW)
DR_i	Ramp down power (KW)
E_{CO2}	Co2 emission rate $\frac{Kg}{KWh}$
E_{NOx}	NOx emission rate $\frac{Kg}{KWh}$
E_{SO2}	SO2 emission rate $\frac{Kg}{KWh}$
E_{PM}	Particle emission rate $\frac{Kg}{KWh}$
$K_{om.}$	Maintenance cost rate coefficient ($\frac{\$}{KWh}$)
η	Efficiency (%)
H	Heat power (KW)
P	Product power (KWh)
C	Cost ($)
ω	Price ($\frac{\$}{KWh}$) or ($\frac{\$}{m^2}$)
U	On/ off state (1 or 0)
$C_{om.}$	Maintenance cost ($)
b.	Battery
g	Natural gas
a	Cost coefficient in ($\frac{\$}{KW^2h}$)

b	Cost coefficient in ($\frac{\$}{KWh}$)
c	Cost coefficient in ($\frac{\$}{h}$)
S^t	Solar radiation in ($\frac{KW}{m^2}$)
t	Time period (h)
SOC^t	State of charge in (KWh)
ch	Charging in (KWh)
dic	Discharging (KWh)
ESS	Energy Storage System
LCV	Low heating value ($\frac{KWh}{m^3}$)
MT	Microturbine
HR	Heat recovery
WT	Wind turbine
PV	Photo voltage panel
SAH	Air Solar Heater
Cce	Cool of electric chiller
Cca	Cool of absorber chiller
EH	Electrical heater
HSS	Heat storage system
MG	Micro grid
CCHP	Compound cool, heat and power
UC	Unit commitment
UG	Utility rid
MINLP	Mixed-Integer Non-Linear Programming
GAMS	General Algebraic Modeling System